



HAL
open science

The tumor microenvironment impairs Th1 IFN γ secretion through alternative splicing modifications of Irf1 pre-mRNA

Antoine Bernard, Christophe Hibos, Corentin Richard, Etienne Viltard, Sandy Chevrier, Sophie Lemoine, Joséphine Melin, Etienne Humblin, Romain Mary, Théo Accogli, et al.

► To cite this version:

Antoine Bernard, Christophe Hibos, Corentin Richard, Etienne Viltard, Sandy Chevrier, et al.. The tumor microenvironment impairs Th1 IFN γ secretion through alternative splicing modifications of Irf1 pre-mRNA. *Cancer Immunology Research*, 2021, 9 (3), pp.324-336. 10.1158/2326-6066.CIR-19-0679 . hal-03834196

HAL Id: hal-03834196

<https://hal.science/hal-03834196>

Submitted on 29 Oct 2022

HAL is a multi-disciplinary open access archive for the deposit and dissemination of scientific research documents, whether they are published or not. The documents may come from teaching and research institutions in France or abroad, or from public or private research centers.

L'archive ouverte pluridisciplinaire **HAL**, est destinée au dépôt et à la diffusion de documents scientifiques de niveau recherche, publiés ou non, émanant des établissements d'enseignement et de recherche français ou étrangers, des laboratoires publics ou privés.

The tumor microenvironment impairs Th1 IFN γ secretion through alternative splicing modifications of *Irf1* pre-mRNA

Antoine Bernard^{1,2,3}, Christophe Hibos^{1,2}, Corentin Richard^{2,3}, Etienne Viltard^{1,2}, Sandy Chevrier³, Sophie Lemoine⁴, Joséphine Melin^{2,5}, Etienne Humblin^{1,2}, Romain Mary^{1,2}, Théo Accogli^{1,2}, Fanny Chalmin¹, Mélanie Bruchard^{1,2,3}, Paul Peixoto⁶, Eric Hervouet⁶, Lionel Apetoh^{1,2}, François Ghiringhelli^{1,2,3}, Frédérique Végran^{1,2,3*}, Romain Boidot^{1,2,3,7*}

Affiliations

¹CRI INSERM UMR1231 “Lipids, Nutrition and Cancer”, Team “CAAdIR”, Dijon, France.

²Faculté des sciences de santé, Université Bourgogne Franche-Comté, Dijon, France

³Centre Georges François Leclerc, Dijon, France

⁴Genomic Platform, Institut de Biologie de l’ENS, Paris, France

⁵LipSTIC LabEx, F-21000, Dijon, France

⁶INSERM UMR1098 “Interactions Hôte-Greffon-Tumeur & Ingénierie Cellulaire et Génique”, Besançon, France

⁷UMR CNRS 6302, Dijon, France

* FV and RB share co-authorship

Running title: TGF β influences alternative splicing of *Irf1* in Th1 cells

* Corresponding authors:

Frédérique Végran : CRI INSERM UMR1231 “Lipids, Nutrition and Cancer”, Team “CAAdIR”, Dijon, France, Email: frederique.vegran@inserm.fr

Romain Boidot: Georges-Francois Leclerc cancer center, Dijon Cedex, France, Email: rboidot@cgfl.fr

Competing interests: The authors declare no conflict of interest.

Funding: We thank “Ligue contre le Cancer de Côte d’Or” and “Ligue contre le Cancer de Saône-et-Loire” for the financial support of this work. We thank “Ligue contre le Cancer” and “Fondation ARC” for the financial support of Antoine Bernard.

Author Contributions: A.B. conducted conceptualization, methodology, investigation, formal analysis and validation of the majority of *in vitro* and *in vivo* experiments, original draft and writing. T.A., M.B., and E.Hu. participated in conceptualization. R.M., F.C., C.H. and E.V. participated in conceptualization and investigation. E.He., P.P., S.C. and J.M. participated in investigation. C.R. participated in bioinformatics analysis, conceptualization, methodology, investigation, validation and formal analysis. S.L. analyzed Nanopore data. L.A. participated in mice resources. F.G. and F.V. participated in supervision, conceptualization, methodology and review & editing. R.B. participated in supervision, conceptualization, methodology, investigation and human sample resources and review & editing.

Abstract

It is clearly established that immune system can affect cancer response to therapy. However, the influence of the tumor microenvironment on immune cells is not completely understood. In this respect, alternative splicing is increasingly described to affect the immune system. Here, we showed that the tumor microenvironment, via a TGF β -dependent mechanism, increased alternative splicing events and induced the expression of an alternative isoform of the IRF1 transcription factor (IRF1 Δ 7) in Th1 cells. We found that the SFPQ splicing factor was responsible for the IRF1 Δ 7 production. We also showed, in both mice and humans, that the IRF1 alternative isoform altered the full-length IRF1 transcriptional activity on the *Il12rb1* promoter, resulting in decreased IFN γ secretion in Th1 cells. Thus, the IRF1 Δ 7 isoform was increased in the tumor microenvironment, and inhibiting IRF1 Δ 7 expression could potentiate Th1 antitumor responses.

Introduction

The tumor microenvironment (TME) is conditioned by complex interactions between malignant and non-malignant cells. Tumor cells mainly secrete immunosuppressive mediators, which contribute to immune surveillance evasion (1,2). The TME consists of a wide variety of cells, immune and not. These cells dynamically communicate amongst themselves, as well as with tumor cells, leading to tumor progression or regression. Transforming growth factor-beta (TGF β) is secreted by malignant and non-malignant cells. This cytokine has an antagonist role in the TME and can either inhibit tumor cell proliferation or disturb activity of antitumor immune cells (3,4). An increasing number of studies show that alternative splicing is involved in immune system differentiation and homeostasis (5,6). This molecular mechanism provides cell flexibility and diversity because it increases the number of protein isoforms from a unique gene. For example, it has been shown that 1319 alternative-splicing events occur upon T-cell receptor (TCR) engagement (7). Alternative splicing allows the immune system to adapt to different environments, such as those within lymph nodes and tumors. Splicing is controlled by a huge protein complex called the spliceosome, which is regulated by splicing factors that control its binding to pre-mRNA (8).

Here, we showed that *Irf1*, encoding crucial transcription factor in Th1 cells IRF1, undergoes alternative splicing in tumors, giving rise to a shortened IRF1 isoform. TGF β was involved in SFPO (splicing factor, proline- and glutamine-rich) splicing factor activation and was responsible for the appearance of the short IRF1 isoform. This isoform acted on the full-length IRF1 transcriptional activity, decreasing *I12rb1* expression and subsequently *Ifn γ* expression. Targeting IRF1 Δ 7 could therefore potentiate Th1-cell antitumor responses.

Methods

Patients and clinical samples

Four tumors samples were kindly provided by the Cancer Center George François Leclerc (Dijon, France), and thirteen healthy donors buffy coats were obtained from Etablissement Français du Sang (Besançon, France). Tumor samples were dissociated using the gentleMACS™ Dissociator (Miltenyi Biotec) in association with Tumor Dissociation Kit (human; 130-095-929, Miltenyi Biotec) or purified with the RosetteSep™ Human CD4⁺ T-cell Enrichment Cocktail (STEMCELL™ Technologies). The study on patient samples was conducted in accordance with the Declaration of Helsinki and approved by the ethics committee of the Centre Georges-François Leclerc (Dijon, France), the Comité Consultatif de Protection des Personnes en Recherche Biomédicale de Bourgogne. Written informed consent was obtained from all patients before enrollment.

Cell lines

Cell lines were cultured at 37°C under 5% CO₂ in Dulbecco's Modified Eagle's Medium (DMEM) (MC-38, B16-F10, LLC1, EL4, 293T, platinum-E) or Roswell Park Memorial Institute medium (RPMI) (for CT-26, 4T1) supplemented with 10% (vol/vol) fetal calf serum (FCS; Lonza), 1% penicillin-streptomycin/amphotericin B (PSA; Gibco), and 4 mM of 4-(2-hydroxyethyl)-1-piperazineethanesulfonic acid (HEPES; Gibco). The MC-38 (Kerafast; ENH204-FP) cell line was derived from C57BL/6 murine colon adenocarcinoma cells. B16-F10 (ATCC; CRL-6475) cell line was derived from a C57BL/6 murine melanoma. LLC1 (ATCC; CRL-1642) cell line was derived from a C57BL/6 murine lung carcinoma. EL4 (ATCC; TIB-39) cell line was derived from a C57BL/6 murine lymphoma. 293T (ATCC; CRL-3216) cell line was derived from a human embryonic kidney. Platinum-E (Plat-E) (Cell Biolabs; RV-101) cell line was generated from 293T cell line. Plat-E cells contain *gag*, *pol*, and *env* genes, allowing retroviral packaging with a single plasmid transfection. The CT-26 (ATCC; CRL-2639) cell line was derived from a BALB/c murine colorectal carcinoma. The 4T1 (ATCC; CRL-2539) cell line was derived from a BALB/c mammary tumor. All cells were routinely tested for Mycoplasma

contamination using the Mycoalert Mycoplasma Detection Kit (Lonza) and were found to be negative.

Mice and tumor model

All the mice were maintained in specific pathogen-free conditions at Dijon Zootechnical Centre, and all experiments followed the guidelines of the Federation of European Animal Science Associations. All animal experiments were approved by the Ethics Committee of Université de Bourgogne (Dijon, France; approved protocol #2212), in accordance with the Federation of Laboratory Animal Science Associations (FELASA). Only females between 6 and 10 weeks of age were used for the experiments. Female C57BL/6 and BALB/c were purchased from Charles River Laboratories (Saint-Germain sur l'Arbresle, France). To induce tumor formation, 8×10^5 MC-38, 8×10^5 CT-26 and 2×10^5 B16-F10 cells were injected subcutaneously into C57BL/6 mice. 8×10^5 CT26 cells were injected subcutaneously into BALB/c mice. Tumor size was measured three times a week with an electronic caliper. After one week, animals were randomized according to tumor size before any treatment to ensure group homogeneity. Mice received three times a week an intraperitoneal injection of IgG1 control antibody (BioXCell; BE0083) or TGF β blocking antibody (BioXCell; BE0057)(100 μ g/mouse). After two weeks, according to our institutional ethical board, animals were sacrificed after anesthetizing. Lymph nodes and spleens were harvested and dissociated using syringe plunger and a 70 μ m filter (Miltenyi Biotec). Red Blood Cell Lysis Buffer (155 mM NH $_4$ Cl, 12 mM NaHCO $_3$ and 0.1 mM EDTA) were added for 2 minutes, and cells were centrifuged (400 \times *g*, 5 minutes) and then suspended in flow cytometry buffer (eBioscience; 00-4222-26) to be labeled. Tumors were harvested and dissociated using the gentleMACS™ Dissociator (Miltenyi Biotec) in association with the Tumor Dissociation Kit (Miltenyi Biotec; 130-096-730). The tumor shreds were filtered using syringe plunger and a 70 μ m filter (Miltenyi Biotec) and centrifuged (400 \times *g*, 5 minutes). Supernatants were harvested for IFN γ ELISA and CD45 $^+$ cells were purified with CD45 (TIL) MicroBeads (Miltenyi Biotec; 130-110-618). CD45 $^+$ cells were labeled in in flow cytometry buffer and analyzed or sorted by flow cytometry.

RNA-sequencing

CD4⁺ T cells were isolated from spleens and tumors of C57BL/6 (MC-38, B16-F10) or BALB/c (CT-26) mice as described above. For RNA-Seq library preparation, total RNA from CD4⁺ T cells was extracted using Trizol. Ribosomal (r)RNA was removed using the Ribo-zero rRNA Removal Kit (Illumina, San Diego, CA, USA). The RINs (RNA integrity numbers) were determined using the TapeStation system (Agilent) and were always above 8. A total of 100 ng of rRNA-depleted RNA was used for the library preparation using the TruSeq Stranded Total RNA Library Prep kit (Illumina) following the manufacturer's instructions. RNA sequencing was performed on NextSeq device (Illumina). The RNA-seq libraries were sequenced with paired-end 75 bp reads. FASTQ files were mapped by using BWA (mm10 version of *Mus Musculus* genome) for Illumina. The analysis was performed by using TopHat for Illumina. Generated files were processed with Cufflinks software to obtain annotated expressed genes in each studied subset. Differential expression between the samples was analyzed with Cuffdiff. Unsupervised hierarchical clustering of samples was performed by using Gene Cluster 3.0 software and viewed with Treeview viewer. Genes were normalized in TPM. All sequencing data are available on the GEO website with the SuperSeries reference: GSE134855.

Nanopore RNA-seq

For RNA-Seq library preparation, total RNA from CD4⁺ T cells cultured with IL12 and with or without TGFβ (3 or 10 ng/mL) was extracted using Trizol (Invitrogen, Carlsbad, CA, USA). The library was prepared using the cDNA-PCR Sequencing Kit (Oxford Nanopore Technologies). Sequencing was performed on GridION device (Oxford Nanopore Technologies). The analysis was performed in collaboration with the Genomic Platform, Institut de Biologie de l'ENS, Paris, France.

Sanger sequencing

Naïve CD4⁺ T cells were isolated from C57BL/6 mouse spleen and differentiated in Th1 cells for 2 hours. Total RNA was extracted using Trizol and was reverse-transcribed into cDNA as described below. cDNA was then amplified by high-fidelity PCR with the Platinum™ Taq DNA Polymerase High Fidelity (Thermo Scientific, 11304011) using primers targeting the exon 6 and exon 7 or exon 6/exon8 junction and intron of *Irf1* (Supplementary Table S1). Sanger sequencing was performed using the Applied Biosystems™ BigDye™ Terminator v3.1 Cycle Sequencing Kit (Thermo Fisher Scientific) and the ABI PRISM 3130xl sequencer (Thermo scientific).

In silico analysis

Intron 6, exon 7, and intron 8 mouse sequences were used to search for splicing factors binding motifs. *In silico* analysis were performed with ENCODE (<https://www.encodeproject.org/>), RBPmap (<http://rbpmap.technion.ac.il/> software), SFmap (<http://sfmap.technion.ac.il/>), and AVISPA (<https://avispa.biociphers.org/galaxy/>) software. The Venn diagrams were generated using the online tool provided by VIB and Ghent University (<http://bioinformatics.psb.ugent.be/webtools/Venn/>).

In vitro T-cell differentiation

Mouse: Naïve CD4⁺ T cells (CD4⁺CD62L⁺) were obtained from spleen and lymph nodes of C57BL/6 wild-type (WT) mice. CD4⁺ T cells were purified from spleen and lymph nodes with anti-CD4 microbeads (Miltenyi Biotec; 130-093-227), then were further sorted as naïve CD4⁺CD62L⁺ T cells using LS column (Miltenyi Biotec; 130-042-401). The purity of the isolated naïve T-cell population routinely exceeded 95%. 5x10⁵ naïve T cells were cultured with anti-CD3 (2 µg/mL) and anti-CD28 (2 µg/mL) in the presence of anti-IFNγ (10 µg/mL) and anti-IL4 (10 µg/mL) to obtain Th0; anti-IL4 (10 µg/mL) and IL12 (10 ng/mL) to obtain Th1; anti-IFNγ (10 µg/mL) and IL4 (10 ng/mL) to obtain Th2; anti-IFNγ (10 µg/mL), anti-IL4 (10 µg/mL), IL6 (20 ng/mL), and TGFβ (2 ng/mL) to obtain Th17; anti-

IFN γ (10 μ g/mL), anti-IL4 (10 μ g/mL), and TGF β (4 ng/mL) to obtain Tregs. Cells were cultured for 2, 24, or 72 hours at 37 °C under 5% CO₂ in RPMI 1640 with 10% (vol/vol) FCS supplemented with sodium pyruvate, 1% penicillin and streptomycin, and 4 mM of HEPES. Anti-CD3 (Armenian Hamster IgG, clone 145-2C11, BE0001-1), anti-CD28 (Armenian Hamster IgG, clone PV-1, BE0015-5), anti-IL4 (Rat IgG1, clone 11B11, BE0045), and anti-IFN γ (Rat IgG1, clone XMG1.2, BE0055) were obtained from BioXcell (West Lebanon, NH, USA), and IL12, IL6, and IL4 were purchased from R&D SYSTEMS and TGF β from Miltenyi Biotec. For *in vitro* treatments, naive CD4⁺ T cells were pre-treated for 1 hour with PI3K inhibitor (0.1 μ M; Merck Chemical France) before beginning the Th1 differentiation with or without TGF β (10 ng/mL).

Human: Naive CD4⁺ T cells (CD4⁺CD62L^{hi}) and differentiated CD4⁺ T-cell subsets (Th1, Th2, Th17) were obtained from human healthy donor buffy coats. Cells were purified by flow cytometry and re-stimulated with plate-bound antibodies against CD3 (1 μ g/mL) and CD28 (5 μ g/mL). 5x10⁵ naive T cells were cultured with anti-CD3 (2 μ g/mL) and anti-CD28 (2 μ g/mL) in the presence of anti-IFN γ (10 μ g/mL) and anti-IL4 (10 μ g/mL) to obtain Th0; anti-IL4 (10 μ g/mL) and IL12 (10 ng/mL) to obtain Th1; anti-IFN γ (10 μ g/mL) and IL4 (20 ng/mL) to obtain Th2; anti-IFN γ (10 μ g/mL), anti-IL4 (10 μ g/mL), IL6 (20 ng/mL), and TGF β (2 ng/mL) to obtain Th17; anti-IFN γ (10 μ g/mL), anti-IL4 (10 μ g/mL), and TGF β (4 ng/mL) to obtain Tregs. Cells were cultured for 2, 24, or 72 hours at 37 °C under 5% CO₂ in RPMI 1640 with 10% (vol/vol) FCS supplemented with sodium pyruvate, 1% penicillin and streptomycin, and 4 mM of HEPES. Anti-CD3 (clone OKT-3; BE0001-2), anti-CD28 (clone 9.3; BE0248), anti-IL4 (clone MP4-25D2; BE0240), and anti-IFN γ (clone B133.5, #BE0055) were obtained from BioXcell (West Lebanon, NH, USA), and IL12, IL6, TGF β , and IL4 were purchased from Miltenyi Biotec.

Retroviral transduction

For retrovirus infection, full-length *Irf1* and the alternatively splice isoform (*Irf1 Δ 7*) were cloned into the pMXs-IRES-GFP retroviral vector (Cell Biolabs). RNA from Th1 cells differentiated from naïve CD4⁺ T cells as described above, was extracted using Trizol and was reverse-transcribed into cDNA as

described below. Fragments were amplified by high-fidelity PCR with C57BL/6 mouse cDNA as template and specific primers (Supplementary Table S1). Ligation of DNA fragments was performed with T4 DNA ligase (Promega; M1801). Insert orientation was determined by PCR and restriction enzyme digestion. Retroviral particles were generated by transfecting the platinum-E cells (Cell Biolabs; RV-101) with Lipofectamine 2000 (Invitrogen; 11668019), according to the manufacturer's instructions. At the same time, naïve CD4⁺ T cells were isolated as described above and cultured in 24-well plates (1x10⁶ / well) coated with anti-CD3 and anti-CD28. After 2 days, 1 mL of fresh virus supernatant was harvested and mixed with 2x10⁶ proliferative CD4⁺ naïve T cells and protamine sulphate (10 µg/mL; APP Pharmaceuticals) in a 24-well coated plate and centrifuged for 60 minutes at 800 × *g* at 32°C. Transduced naïve CD4⁺ T cells were collected after 2 days, and cell-sorted with a FACSAria™ Cell Sorter (BD Bioscience) according to GFP expression. GFP⁺ cells used for intracellular staining were fixed in 2% PFA. Otherwise, GFP⁺ cells were differentiated as described above, and after 1 or 3 days, the cells were collected for PCR and ELISAs.

Reverse transcription PCR and quantitative PCR analysis

Total RNA from differentiated CD4⁺ T cells was extracted using Trizol. In total, 300 ng of RNA was reverse-transcribed into cDNA using M-MLV reverse transcriptase (28025-013, Invitrogen), Random Primers, and RNaseOUT inhibitor (10777-019, Invitrogen). cDNAs were quantified by real-time PCR using a Power SYBR Green Real-time PCR kit (4367659, Life technologies) on a StepOne detection system (Thermo Scientific). Relative mRNA levels were determined using the Δ Ct method. Values were expressed relative to β -actin unless otherwise specified. The sequences of the oligonucleotides used are described in Supplementary Table S1.

ELISAs

After polarization for 72 hours, cell culture supernatants of different tumor cell lines (1/100 dilution) were assayed by ELISA for mouse IFN γ (BD Biosciences; 555138). IFN γ concentration was also

assessed in tumor shreds (pure). An ELISA for mouse TGF β (R&D SYSTEMS; DY1679-05) was performed according to the manufacturer's protocol.

Western blotting and immunoprecipitation assays

Differentiated CD4⁺ T cells were lysed in boiling buffer (1% SDS, 1 mM sodium orthovanadate, and 10 mM Tris (pH 7.4)) containing protease inhibitor cocktail (Roche; 11697498001) for 20 minutes at 4°C. Cell lysates were subjected to sonication (10 seconds at 10% intensity), and protein concentration was assessed using the Bio-Rad DC Protein Assay Kit (5000112, Bio-Rad). Proteins were then denatured, loaded, and separated on SDS-PAGE and transferred on nitrocellulose membranes (Schleicher & Schuell). After blocking with 5% non-fat milk in PBS containing 0.1% Tween 20 (PBST), membranes were incubated overnight with primary antibody diluted (1 μ g/mL) in PBST containing 5% BSA, washed, and incubated for 1 hour with secondary antibody (1/10000) diluted in PBST-5% non-fat milk. After additional washes, membranes were incubated for 1 minute with luminol reagent (Santa Cruz Biotechnology). The following antibodies were used for in immunoblotting. Primary antibodies: rabbit anti-IRF1 N-terminal region was purchased from Aviva systems biology, and mouse anti-HSC70 (B-6) was purchased from Santa Cruz Biotechnology. Secondary antibodies: peroxidase AffiniPure goat polyclonal anti-rabbit IgG (H+L)(Jackson ImmunoResearch), and peroxidase AffiniPure goat polyclonal anti-mouse IgG (H+L) (Jackson ImmunoResearch).

Chromatin immunoprecipitation assay

Chromatin isolation and shearing were performed with the truChIPTM Chromatin Shearing Kit (Covaris) using a Focused-Ultrasonicator M220 device (Covaris). A chromatin immunoprecipitation (ChIP) assay was performed with the CHIP-IT kit (Active Motif Europe, Rixensart, Belgium) according to the manufacturer's instructions. A total of 7 μ g of DNA were immunoprecipitated with 3 μ g of anti-histidine or anti-YFP (Thermo Scientific), or 3 μ g of negative control immunoglobulin at 4°C

overnight. After chromatin elution, cross-links were reversed, and samples were analyzed by quantitative PCR as described above. The sequences of the oligonucleotides used are described in Supplementary Table S1.

RNA immunoprecipitation

RNA immunoprecipitation (RIP) was performed with Magna RIP™ RNA-Binding Protein Immunoprecipitation Kit according to the manufacturer's instructions. RNA was immunoprecipitated with 5 µg of anti-SFPQ (Abcam). RNA was reverse-transcribed into cDNA and analyzed by quantitative PCR as previously described.

siRNA transfection

siRNA knockdown experiments were performed in mouse and human with validated controls, or *Irf1*-, *Irf1Δ7*-, *Sfpq* (mouse)-specific siRNAs (Life Technologies). In brief, naive CD4⁺ T cells were transfected with Transit-TKO Transfection Reagent (MIR2154, Mirus) according to the manufacturer's instructions for 24 hours and then differentiated as previously described. The sequences of the siRNAs used are described in Supplementary Table S1

Promoter-activity reporter assay

The *I12rb1*-luc luciferase construct was obtained by inserting 154 base pairs of *I12rb1* mouse promoters in the multicloning site of the pGL3 basic vector (Promega, Charbonnières, France). Fragments were amplified by high-fidelity PCR with C57BL/6 mouse DNA as the template and specific primers (Supplementary Table S1). 1×10^5 Human 293T cells were transiently transfected for 48 hours with the pSV-β-galactosidase (Promega) reporter plasmid and the pcDNA3.1/CT-GFP-TOPO-IRF1 (Thermo Scientific), pcDNA3.1/CT-GFP-TOPO-IRF1Δ7 using Lipofectamine 2000 (Invitrogen). Luciferase was measured using the Dual Glo Luciferase Assay System (Promega; E2920) according to

the manufacturer's instructions. Firefly luciferase was measured with an EnVision 2105 Multimode Plate Reader (PerkinElmer).

Immunofluorescence (IF)

1×10^6 of CD4⁺ T cells per condition were used. Cells were washed, fixed for 10 minutes at room temperature with 4% paraformaldehyde (PFA) and permeabilized for 10 minutes on ice with methanol (100% glacial) and saturated for 45 minutes with a buffer of 5% BSA and 0.2% Triton X-100 (Sigma-Aldrich) in PBS. Samples were then incubated overnight at 4°C with primary antibodies (identified below and detailed in Supplementary Table S1), diluted in 5% BSA buffer. Cells were washed two times with a solution of 0.05% Tween 20 in PBS (PBS-Tween) and incubated for 1 hour at room temperature with the secondary antibody (identified below and detailed in Supplementary Table S1) diluted in the IF blocking buffer. Cells were then washed two times with PBS-Tween solution and two times with ultrapure water. Stained cells resuspended in ultrapure water were dropped off on microscopy slides (Superfrost Ultra Plus®, ThermoFisher Scientific) and incubated at room temperature in dark until water evaporation. Dried slides were mounted with a drop of Mounting Medium containing DAPI (Molecular Probes) and covered with a cover slip (Knittelglass). Slides were imaged with a charge-coupled device–equipped upright microscope (Zeiss) and 40x or 63x objective with a numerical aperture of 1.4 using Zeiss ApoTome system (for 63x magnification). Images were analyzed with ZEN lite (ZEISS). Threshold were defined according to negative control fluorescence (IgG). The following antibodies were used for IF. Primary antibodies: rabbit anti-SFPQ (Abcam); Secondary antibodies: goat polyclonal anti-rabbit IgG (H+L) Cross-Adsorbed Alexa Fluor 568 (ThermoFisher Scientific).

FLIM-FRET

The IRF1-YFP and IRF1Δ7-CFP constructs were obtained by inserting 819 bp of *Irf1Δ7* in the multiple cloning site of the mVenus C1 vector (Addgene) and by inserting 990 bp of *Irf1* into mCerulean C1

(Addgene) respectively. Fragments were amplified by high-fidelity PCR with C57BL/6 mouse cDNA as template and specific primers Supplementary Table S1. Fluorescence lifetime imaging (FLIM) was performed, and images were collected using a time-correlated single-photon counting (TCSPC) module (PicoQuant) on a Nikon A1-MP scanning microscope. Imaging was carried out with a $\times 60$ Apo IR objective (NA: 1.27, Water Immersion, Nikon). Two-photon excitation at 820 nm was provided by an IR laser (Chameleon, Coherent) that delivered femtosecond pulses at a repetition rate of 80 MHz. Fluorescence emission of CFP was collected through a FF01-494/20 band-pass emission filter (Semrock) using a single-photon avalanche diode detector. TCSPC lifetime recording was performed over 200 temporal channels (final resolution 0.64 ps). We performed a global lifetime analysis on regions of interest of the FLIM images using SymPhoTime software (PicoQuant). The fluorescence lifetimes were calculated by fitting the tail of the fluorescence decay with a biexponential model.

Flow cytometry

To phenotype and sort distinct mouse CD4⁺ T-cell populations by flow cytometry, dissociated lymph nodes, spleens, and MC-38 tumors were analyzed. To phenotype and sort distinct human CD4⁺ T-cell populations by flow cytometry, colorectal tumors and healthy donor buffy coats were analyzed. For surface staining, CD4⁺ T cells were stained with different antibodies (Supplementary Table S1) in Flow Cytometry Staining Buffer (eBioscience) and Brilliant Stain Buffer (BD Biosciences) for 15 minutes at room temperature. For intracellular cytokine staining, CD4⁺ T cells were stimulated for 3 hours at 37°C in culture medium containing PMA (50 ng/mL; Sigma), ionomycin (1 mg/mL; Sigma), and monensin (GolgiStop; 1 mg/mL; BD Biosciences). Cells were stained in Flow Cytometry Staining Buffer (eBioscience) and Brilliant Stain Buffer (BD Bioscience) with different antibodies Supplementary Table S1. FOXP3 intracellular staining was carried out according to manufacturer's protocol using the fixation/permeabilization solution (eBioscience). All events were acquired by a BD LSRII™, FACSCanto™ 10-Color or a LSRFortessa™ cell analyzer, or sorted by a FACSAria™ Cell Sorter (BD

Bioscience) equipped with BD FACSDiva software (BD Biosciences). Data were analyzed using Flowlogic or FlowJo software.

Quantification and statistical analysis

Results are shown as mean with SD or SEM. Datasets were compared using unpaired Mann-Whitney test, Kruskal-Wallis test, one/two-way ANOVA test when appropriate. Statistical calculations were done using GraphPad Prism 7. All *P* values were two-tailed. Ns, not significant; **P*<0.05, ***P*<0.01, ****P*<0.001, and *****P*<0.0001.

Results

Tumor microenvironment impacts CD4⁺ T-cell alternative splicing

First, we tested the pattern of alternative splicing in bulk of CD4⁺ T cells from spleens or tumors by RNA-sequencing (Supplementary Figure S1). We observed a global increase in splicing events in tumors compared to spleen (Figure 1A). GSEA analysis of genes with a higher expression in tumors showed a significant enrichment in splicing factor gene expression (Figure 1B). When comparing transcriptomic profiles of bulk CD4⁺ T cells from spleens and tumors, we observed a clear impact on Th1- (Figure 1C), Th2-, Th17-, and Treg-related gene expression (Supplementary Figure S1B). Th1 cell presence in tumors is reported as a good prognosis indicator (9); therefore, we wondered whether TME-induced alternative splicing modifications had an impact on Th1 master controller genes *Tbx21* and *Irf1*. To determine if *Tbx21* and *Irf1* pre-mRNA were alternatively spliced in Th1 cells, we generated Th1 CD4⁺ T cells *in vitro* and analyzed both *Tbx21* and *Irf1* by PCR and Sanger sequencing. We detected an *Irf1*-spliced isoform in which exon 7 had been excluded (*Irf1Δ7*), whereas no splice variant was found for *Tbx21* mRNA (Supplementary Figure S2A). In addition to exon 7 skipping, we identified the inclusion of intron 8 together with an in-phase stop codon by Sanger sequencing (Supplementary Figure S2B) and through Nanopore sequencing (Supplementary Figure S2C), avoiding

nonsense-mediated decay degradation and enabling mRNA stabilization (Supplementary Figure S2D). Quantification by digital PCR revealed that the strongest expression level of *Irf1* was detected 2 hours after Th1 differentiation start (Figure 1D), and 4 hours for *Irf1Δ7* mRNA (Figure 1E). After 4 hours of differentiation, *Irf1Δ7* mRNA represented almost 20% of the *Irf1* gene expression (Figure 1F). In different subsets of *in vitro*-differentiated helper T cells, we observed that *Irf1* mRNA was 56%, 30%, and 78% less expressed in Th2, Th17, and Treg respectively, than in Th1 cells, and that *Irf1Δ7* mRNA was 83%, 46%, and 87% less expressed in Th2, Th17, and Treg respectively, than in Th1 cells (Supplementary Figure S3). We confirmed the expression of *Irf1* (Figure 1G) and *Irf1Δ7* mRNA (Figure 1H) in *in vivo* Th1 cells isolated from spleens (Supplementary Figure S4). To determine whether the short form of IRF1 was detected at the protein level, we performed Western blotting using an antibody targeting the protein N-terminal domain. We detected two proteins of 37 and 35 KDa, corresponding to the predicted sequence molecular weight (Supplementary Figure S5), indicating that both proteins were expressed (Figure 1I). Collectively, these findings indicated that IRF1, a master controller of Th1 cell differentiation, could be affected by alternative splicing at the mRNA level, giving rise to another stable isoform that is translated in Th1 cells.

TGFβ affects *Irf1Δ7* isoform appearance

TGFβ is one of the most common cytokines found in TME (10) and is described as modifying alternative splicing in cancer cells (11). By comparing the transcriptomic profiles of CD4⁺ T cells isolated from spleens and tumors, we underlined TGFβ-related gene enrichment in tumor CD4⁺ T cells (Figure 2A-B), whereas no enrichment was found with IL6 (Supplementary Figure S6A), another cytokine in TME (12). By dosing TGFβ in the tumor shred of different cell lines (Figure 2C) and directly in the cell culture supernatant (Supplementary Figure S6B), we validated the secretion of this cytokine by different mouse tumor cell lines, CT-26 and MC-38. The amount of TGFβ was higher in tumor shreds than in supernatants (except for EL4 cells), suggesting that TGFβ could be secreted by tumor cells and tumor-infiltrating cells. On this basis, we hypothesized that TGFβ from TME could

have an impact on Th1 CD4⁺ T-cell alternative splicing and consequently on *Irf1Δ7* isoform expression. To test this hypothesis, naïve CD4⁺ T cells were cultured for 2 hours with IL12 and increasing doses of TGFβ and then differentiated for 24 hours with IL12 only (Supplementary Figure S7). Using Nanopore sequencing, we confirmed that TGFβ affected *Irf1* mRNA exon 7 inclusion at 2 hours (Figure 2D), and we also noted an increase in intron 8 inclusion (Figure 2E). After 2 hours of TGFβ exposure, we did not observe, by PCR, differences in *Irf1* mRNA expression (Figure 2F) but did see an increase in *Irf1Δ7* mRNA expression, indicating an increase in exon 7 exclusion (Figure 2G), confirming the Nanopore data. Thus, in these conditions, the fold-change ratio was in favor of *Irf1Δ7* mRNA (Figure 2H). After 24 hours of Th1 differentiation without TGFβ, *Tbx21* (Figure 2I) and *Foxp3* (Figure 2J) mRNA expression remained unchanged, while *I12rb1* (Figure 2K) and *Ifng* mRNA (Figure 2L) expression were decreased in a dose-dependent manner. To confirm the involvement of TGFβ in *Irf1* mRNA alternative splicing, we monitored tumor growth in MC-38 (TGFβ-producing)-bearing C57BL/6 mice treated with TGFβ-blocking antibody or control (Supplementary Figure S8A). We observed inhibition of tumor growth upon TGFβ targeting compared to controls (Supplementary Figure S8B). After sorting Th1 cells from spleens and tumors from anti-TGFβ-treated and untreated mice, we analyzed the *Irf1Δ7/Irf1* ratio by RT-qPCR. We observed an increase in *Irf1Δ7* mRNA expression in Th1 cells from tumors compared to those from spleens in controls (Figure 2M). In parallel, we observed a significant decrease in *Irf1Δ7* mRNA in tumors when mice were treated with TGFβ-blocking antibody (Figure 2M). We also found a significant increase in IFNγ in tumors from mice treated with TGFβ-blocking antibody (Figure 2N). This observation was validated by an increase in CD4⁺IFNγ⁺ cells in tumors from mice treated with TGFβ-blocking antibody (Figure 2O, Supplementary Figure S9A and-S9B). We observed no significant differences in CD4⁺Foxp3⁺ cells in blocking antibody-treated and -untreated tumors (Figure 2P, Supplementary Figure S9B). We obtained similar results in BALB/c mice injected with CT-26 cells in terms of tumor growth, *Irf1Δ7* mRNA expression, and IFNγ secretion (Supplementary Figure S10A-C). Together, these data showed that TGFβ was able to induce *Irf1Δ7* isoform appearance *in vitro* and *in vivo*.

SFPQ splicing factor regulates *Irf1* pre-mRNA alternative splicing

Because TGF β impacted *Irf1* pre-mRNA alternative splicing, we wondered what could be the mechanism at play. Using transcriptomic analysis of CD4⁺ T cells isolated from spleens and tumors, we observed 26 splicing factor genes overexpressed in CD4⁺ T cells infiltrating tumors (Figure 3A). Through *in silico* analysis (Supplementary Figure S11-S14), we analyzed intron 6, exon 7, and intron 7 of *Irf1* pre-mRNA sequence to identify splicing factor binding sites. By crossing RNAseq results and *in silico* results, we identified SFPQ as the splicing factor potentially involved in *Irf1 Δ 7* mRNA expression (Figure 3B). Transcriptomic analysis of Th1 cells isolated from spleens and B16-F10 tumors validated SFPQ and hnRNPF (heterogeneous nuclear ribonucleoprotein F) in *Irf1 Δ 7* mRNA expression (Supplementary Figure S215A and S15B). To determine whether any splicing factors were involved in TGF β -induced exon 7 alternative splicing, naïve CD4⁺ T cells were cultured for 2 hours with TGF β and IL12. We then analyzed the transcriptional expression of *Hnrnpf*, *Sfpq*, and *Hnrnp1* (another splicing factor upregulated in tumors but not selected *in silico*). Only *Sfpq* mRNA expression was significantly increased, whereas neither *Hnrnpf* nor *Hnrnp1* mRNA was statistically impacted by TGF β pre-treatment (Figure 3C). SFPQ activity is described to be regulated by the PI3K/AKT pathway, leading to its fixation on CD45 mRNA (13). After naïve CD4⁺ T-cell treatment using IL12 and TGF β , we observed, by immunofluorescence, that SFPQ expression in the nucleus was increased in response to TGF β (Figure 3D). GSEA analysis showed a positive enrichment of PI3K/AKT pathway-related genes in tumors (Figure 3E). To confirm the involvement of PI3K/AKT pathway, we pretreated IL12- and TGF β -incubated naïve CD4⁺ T cells with a PI3K/AKT pharmacological inhibitor. This completely abolished the increase of *Irf1 Δ 7* mRNA expression in response to TGF β (Figure 3F). To further study the effect of TGF β in SFPQ activity, we analyzed SFPQ interaction on *Irf1* mRNA upon mRNA immunoprecipitation. We observed that TGF β increased the binding of SFPQ to *Irf1 Δ 7* mRNA (Figure 3G). When we transfected Th1 cells with an siRNA-targeting *Sfpq* (Supplementary Figure S16A-C), we observed a decrease in *Irf1 Δ 7* mRNA expression (Figure 3H), whereas *Irf1* was not impacted

(Supplementary Figure S16D). These data suggest the involvement of SFPQ in *Irf1Δ7* mRNA appearance, through PI3K/AKT pathway activation in response to TGFβ.

IRF1Δ7 impairs Th1-cell activity

After seeing TGFβ's effects on *Irf1Δ7* occurrence, we focused on determining if this isoform may have a direct effect in Th1 activity. Using siRNA, we saw that *Irf1* depletion (Supplementary Figure S16E) associated with a decrease in *Il12rb1* and *Ifng* mRNA expression. *Irf1Δ7* (Supplementary Figure S16F) and *Sfpq* (Supplementary Figure S16A-C) mRNA depletion associated with an increase in *Il12rb1* and *Ifng* mRNA expression (Figure 4A-D). *Irf1Δ7* and *Sfpq* mRNA depletion induced higher IFNγ secretion (Figure 4E). In contrast, overexpression of IRF1Δ7 using a retroviral strategy (Figure 4F) inhibited Th1 cell differentiation, as demonstrated by the decreased production of both *Il12rb1* and *Ifng* mRNA (Figure 4G-H). Th1 IFNγ⁺ cells (Figure 4I, Supplementary Figure S17) and IFNγ secretion (Figure 4J) were also decreased by IRF1Δ7 overexpression.

To understand, how IRF1Δ7 impacted *Il12rb1* and *Ifng* expression in Th1 cells, we first performed a ChIP analysis to determine whether IRF1Δ7 could interact with DNA. We used 293T cells transfected with either *Irf1* or *Irf1Δ7* or both expression plasmids tagged with histidine or YFP. Cells were transfected with *Il12rb1* plasmid containing 154 basepairs of the promoter region and 18 basepairs downstream of the transcription-initiation site known to be the DNA binding site of IRF1 (14). We confirmed an interaction of IRF1 with *Il12rb1* promoter but no interaction of IRF1Δ7 was observed (Figure 4K). When both IRF1 isoforms were present, we observed a disruption of IRF1 interaction with *Il12rb1* promoter (Figure 4K). To confirm the negative effect of IRF1Δ7 on IRF1 transcriptional activity, we cloned *Il12rb1* promoter into a luciferase reporter plasmid. *Il12rb1* reporter plasmid was transfected either alone or with an *Irf1*-expressing plasmid with an increasing yield of *Irf1Δ7*-expressing plasmid. IRF1 alone significantly activated the *Il12rb1* promoter, as evidenced by an increase luciferase activity. The activity of the *Il12rb1* promoter, due to the IRF1 isoform, was

decreased in an IRF1 Δ 7 dose-dependent manner (Figure 4L). We therefore hypothesized that IRF1 Δ 7 could interact with IRF1 and prevent its binding to DNA. To address this question, we performed a FRET assay in 293T cells transfected with both IRF1 and short-expression plasmids tagged with CFP and YFP respectively. Our data indicated that the donor fluorescence (CFP) decreased faster when both isoforms were expressed together (Figure 4M), indicating a high proximity (<5nm) between the different isoforms. These data suggested a potential interaction between IRF1 and IRF1 Δ 7. Taken together, these data demonstrated that IRF1 Δ 7 reduced Th1 activity by decreasing DNA binding of IRF1 to the *Il12rb1* promoter.

IRF1 Δ 7 is present in human Th1 cells and modulates their activity

We then asked whether inhibiting the impact of IRF1 alternative splicing isoform was transposable to human cells. We validated the exon 7 exclusion in T-helper cells *in vitro* after 1 hour of differentiation (Supplementary Figure S18). This isoform was similar to the *Irf1 Δ 7* identified in mice. Expression of the short *IRF1* mRNA isoform, detected by qPCR, was similar among Th1, Th2, and Th17 cells (Figure 5A). *In vivo* expression of *IRF1 Δ 7*, detected by qPCR, was significantly higher in Th1 and lower in Th17 cells compared to naïve T cells (Figure 5B, Supplementary Figure S19). Because IRF1 Δ 7 impaired Th1 differentiation in mice, we wondered whether this *IRF1* isoform could still have an effect on human Th1 differentiation. Targeting this isoform using siRNA (Supplementary Figure S20A-C), led to an increase in *Il12rb1* and *Ifng* mRNA expression (Figure 5C-D), an increase in IFN γ ⁺ cells (Figure 5E, Supplementary Figure S20D), and an increased IFN γ secretion evaluated by ELISA (Figure 5F). To determine if TGF β also had an effect on the alternative splicing profile of *IRF1* mRNA in human Th1 cells, naïve CD4⁺ T cells or *ex vivo* Th1 cells obtained from healthy blood donors were cultured for 1 hour with IL12 and increasing doses of TGF β and then differentiated for 24 hours after TGF β withdrawal (Figure S21). We did not note any differences in *IRF1* mRNA expression (Figure 5G and H), but did observe an increase in *IRF1 Δ 7* mRNA (Figure 5I-J). Thus, in these conditions, the fold-change ratio was in favor of *IRF1 Δ 7* mRNA (Figure 5K-L). After 24 hours of Th1 differentiation without TGF β ,

IFNG expression (Figure 5M-N) was decreased in a dose-dependent manner. To attest the effect of the TME on alternative splicing profile of *IRF1* mRNA, we sorted Th1 cells from healthy blood donors and from colon tumors, and observed a significant increase in the *IRF1Δ7* isoform in Th1 cells isolated from tumors (Figure 5O). Together, these data emphasize that the short *IRF1* mRNA isoform is also expressed in different human T-helper cells, particularly Th1 cells, where it down-modulates Th1 activation, as was observed in mouse models.

Discussion

Alternative splicing of pre-mRNA provides a higher level of genetic diversity and complexity by increasing the number of protein forms of the same gene (15). This molecular phenomenon provides a way respond and adapt to a given environment (16). It is now well-recognized that the immune system is an integral part of the disrupted microenvironment in tumors (17). Our report showed an impact of TME in CD4⁺ Th1 cells. By comparing the same cells isolated from spleen or tumors, we observed a global alternative splicing increase in CD4⁺ T cells in tumors. Among them, we focused on Th1 cells, in which we identified a new splicing isoform of IRF1, a master controller of Th1 differentiation. From our results we identified an isoform lacking exon 7 and included a part of intron 8 containing an in-frame stop codon.

TGFβ is the most common cytokine found in TME (18). It can be secreted both by tumor cells and by non-tumor cells, like Tregs. TGFβ immunosuppressive mechanisms are not fully understood. Studies suggest that TGFβ signaling pathway in tumor cells has an important impact on alternative splicing of CD44, favoring epithelial-to-mesenchymal transition and metastasis (11). Here, our data showed that targeting TGFβ with blocking antibodies during tumor growth induced a decrease in *Irf1Δ7* expression and an increase in IFNγ secretion in tumors. *In vitro*, we observed that increasing TGFβ concentration in presence of IL12 for 2 hours, corresponding to the peak level of *Irf1* expression,

increased *Irf1Δ7* expression. This treatment did not affect the expression of *Tbx21*, the master regulator of Th1 cells, and did not induce the expression of *Foxp3*, the key transcription factor of Treg differentiation. However, we saw a decrease in *Il12rb1* expression, a gene whose expression is under IRF1 control, and also a decrease in *Ifnγ* expression in a dose-dependent manner. Thus, *Irf1* pre-mRNA alternative splicing could exacerbate TGFβ immunosuppressive effects on Th1 cells.

Splicing factors are key regulators of spliceosome activity because they modulate its binding to pre-mRNA (19). Their activity is finely regulated by extracellular signals, but underlying molecular mechanisms remain unclear (20). In human T cells, it has been reported that antigen stimulation induces skipping of 3 exons of CD45 to produce CD45RO (13), and the shorter isoform is less active than the full-form and tempers T-cell activation. The splicing factor involved in this phenomenon is SFPQ. When phosphorylated by GSK3, SFPQ stays inactive because of its sequestration by TRAP150. Our results showed that SFPQ is the only splicing factor overexpressed in the TME that could be specific to *Irf1* pre-mRNA splicing. Indeed, *Sfpq* had a significant expression increase when cells were treated with TGFβ. We also found that SFPQ interacted more with *Irf1* mRNA when naïve CD4⁺ T cells were exposed to IL12 and TGFβ. When SFPQ was targeted by siRNA, *Irf1Δ7* mRNA expression was decreased, and the inhibition of PI3K (controlling GSK3 activity) activity with a pharmacologic inhibitor, completely canceled the effect of TGFβ on *Irf1Δ7* mRNA expression. Nevertheless, the full mechanism leading to SFPQ activation by this cytokine remains to be fully decrypted. However, it is known that SR (serine- and arginine-rich) proteins (21) and hnRNPs (22) activity are modulated by the PI3K/AKT pathway. Thus, the disruptions of alternative splicing mediated by TGFβ most likely impact some splicing factors, and SFPQ is responsible for *Irf1Δ7* production.

The transcription factor IRF1 has been identified to regulate the expression of a large number of genes in different cell types (23-26). Concerning immune cells, Th1 lymphocyte development is supported by IRF1 through the transcriptional control of *Il12rb1* gene expression (14). In Tregs, IRF1

negatively regulates *Foxp3* expression (27). However, alternative splicing of IRF1 is still largely underexplored, especially in immune cells. Nevertheless, experiments using normal and malignant human cervical tissue samples reveals five IRF1 variants lacking some combinations of exons 7, 8, and 9 (28). The study also showed that these variants were able to inhibit the transcriptional activity of IRF1 full-form. In this context, we observed that *IRF1Δ7* had a negative impact on Th1 cell activity. Thus, *IRF1Δ7* impaired IRF1 transcriptional activity by preventing its interaction with the *IL12rb1* promoter, probably by sequestration. Th1 cells are known to have potent antitumor properties by their faculty to secrete a large amount of IFN γ , a source of activation of other antitumor cells like CD8⁺ T cells (29). We found *in vitro* that in the absence of the short isoform of IRF1, Th1 cells can secrete even more IFN γ , which might potentiate their antitumor activity.

RNA-sequencing has shown that around 95% of human genes are alternatively spliced (30). However, few studies have analyzed the impact of alternative splicing on human immune system homeostasis (31). Our study indicated that, as in mice, an IRF1 alternative isoform without the exon 7 exists in humans. When we targeted the *IRF1Δ7* form, we observed an increase in *IFNG* expression that tended towards exacerbated antitumor activity. We noted that, when compared to Th1 cells from healthy donors' blood, Th1 cells from tumors had a higher expression of *IRF1Δ7*. Hence, a short form of *IRF1* was also expressed in human Th1 cells and possessed similar negative effects on Th1 cell activity, as was observed in mouse models.

In summary, we have shown that a short isoform of IRF1 lacking exon 7 is expressed in Th1 cells, and that its expression is increased in the TME *via* a TGF β -dependent mechanism. We also found that *IRF1Δ7* had a negative impact in IRF1 isoform transcriptional activity in Th1 cells. Targeting *IRF1Δ7* could therefore potentiate Th1 cell antitumor responses.

Acknowledgments

This work was funded by the Fondation ARC pour la recherche sur le cancer and the Ligue Nationale contre le Cancer. Authors would like to thank to the Plateforme de Cytométrie (<http://www.cytometrie-dijon.fr>) (Anabelle Sequeira, Dijon, France) for providing reagents and access to their cytometers, the Centre de Zootechnie (<http://recherche.u-bourgogne.fr/potentiel-de-recherche/plateformes-technologiques/centre-de-zootechnie.html>) (Valérie Saint-Giorgio, Dijon, France) for providing animal bred facilities and devices to perform *ex vivo* and *in vivo* experiments and the DImaCell Imaging Facility for the use of FLIM microscopy and for technical assistance. DImaCell equipments are funded by the Regional Council of Bourgogne - Franche Comté and the "Fonds Européen de DEveloppement Régional (FEDER)". Finally, authors thank Isabel Grégoire, CGFL for manuscript editing.

References

1. Anderson KG, Stromnes IM, Greenberg PD. Obstacles Posed by the Tumor Microenvironment to T cell Activity: A Case for Synergistic Therapies. *Cancer Cell* **2017**;31(3):311-25 doi 10.1016/j.ccell.2017.02.008.
2. Hanahan D, Coussens LM. Accessories to the crime: functions of cells recruited to the tumor microenvironment. *Cancer Cell* **2012**;21(3):309-22 doi 10.1016/j.ccr.2012.02.022.
3. Colak S, Ten Dijke P. Targeting TGF-beta Signaling in Cancer. *Trends Cancer* **2017**;3(1):56-71 doi 10.1016/j.trecan.2016.11.008.
4. Ikushima H, Miyazono K. TGFbeta signalling: a complex web in cancer progression. *Nat Rev Cancer* **2010**;10(6):415-24 doi 10.1038/nrc2853.
5. Baralle FE, Giudice J. Alternative splicing as a regulator of development and tissue identity. *Nat Rev Mol Cell Biol* **2017**;18(7):437-51 doi 10.1038/nrm.2017.27.
6. Yabas M, Elliott H, Hoyne GF. The Role of Alternative Splicing in the Control of Immune Homeostasis and Cellular Differentiation. *Int J Mol Sci* **2015**;17(1) doi 10.3390/ijms17010003.
7. Butte MJ, Lee SJ, Jesneck J, Keir ME, Haining WN, Sharpe AH. CD28 costimulation regulates genome-wide effects on alternative splicing. *PLoS One* **2012**;7(6):e40032 doi 10.1371/journal.pone.0040032.
8. Shi Y. Mechanistic insights into precursor messenger RNA splicing by the spliceosome. *Nat Rev Mol Cell Biol* **2017**;18(11):655-70 doi 10.1038/nrm.2017.86.
9. Pages F, Galon J, Dieu-Nosjean MC, Tartour E, Sautes-Fridman C, Fridman WH. Immune infiltration in human tumors: a prognostic factor that should not be ignored. *Oncogene* **2010**;29(8):1093-102 doi 10.1038/onc.2009.416.
10. Trapani JA. The dual adverse effects of TGF-beta secretion on tumor progression. *Cancer Cell* **2005**;8(5):349-50 doi 10.1016/j.ccr.2005.10.018.
11. Tripathi V, Sixt KM, Gao S, Xu X, Huang J, Weigert R, *et al.* Direct Regulation of Alternative Splicing by SMAD3 through PCBP1 Is Essential to the Tumor-Promoting Role of TGF-beta. *Mol Cell* **2016**;64(5):1010 doi 10.1016/j.molcel.2016.11.025.
12. Johnson DE, O'Keefe RA, Grandis JR. Targeting the IL-6/JAK/STAT3 signalling axis in cancer. *Nat Rev Clin Oncol* **2018**;15(4):234-48 doi 10.1038/nrclinonc.2018.8.
13. Heyd F, Lynch KW. Phosphorylation-dependent regulation of PSF by GSK3 controls CD45 alternative splicing. *Mol Cell* **2010**;40(1):126-37 doi 10.1016/j.molcel.2010.09.013.
14. Kano S, Sato K, Morishita Y, Vollstedt S, Kim S, Bishop K, *et al.* The contribution of transcription factor IRF1 to the interferon-gamma-interleukin 12 signaling axis and TH1 versus TH-17 differentiation of CD4+ T cells. *Nature immunology* **2008**;9(1):34-41 doi 10.1038/ni1538.
15. Nilsen TW, Graveley BR. Expansion of the eukaryotic proteome by alternative splicing. *Nature* **2010**;463(7280):457-63 doi 10.1038/nature08909.
16. El Marabti E, Younis I. The Cancer Spliceome: Reprogramming of Alternative Splicing in Cancer. *Front Mol Biosci* **2018**;5:80 doi 10.3389/fmolb.2018.00080.
17. Binnewies M, Roberts EW, Kersten K, Chan V, Fearon DF, Merad M, *et al.* Understanding the tumor immune microenvironment (TIME) for effective therapy. *Nature medicine* **2018**;24(5):541-50 doi 10.1038/s41591-018-0014-x.
18. Papageorgis P, Stylianopoulos T. Role of TGFbeta in regulation of the tumor microenvironment and drug delivery (review). *International journal of oncology* **2015**;46(3):933-43 doi 10.3892/ijo.2015.2816.
19. Matera AG, Wang Z. A day in the life of the spliceosome. *Nat Rev Mol Cell Biol* **2014**;15(2):108-21 doi 10.1038/nrm3742.
20. Tarn WY. Cellular signals modulate alternative splicing. *J Biomed Sci* **2007**;14(4):517-22 doi 10.1007/s11373-007-9161-7.
21. Zhou Z, Fu XD. Regulation of splicing by SR proteins and SR protein-specific kinases. *Chromosoma* **2013**;122(3):191-207 doi 10.1007/s00412-013-0407-z.

22. Doltra A, Stawowy P, Dietrich T, Schneeweis C, Fleck E, Kelle S. Magnetic resonance imaging of cardiovascular fibrosis and inflammation: from clinical practice to animal studies and back. *Biomed Res Int* **2013**;2013:676489 doi 10.1155/2013/676489.
23. Kim PK, Armstrong M, Liu Y, Yan P, Bucher B, Zuckerbraun BS, *et al.* IRF-1 expression induces apoptosis and inhibits tumor growth in mouse mammary cancer cells in vitro and in vivo. *Oncogene* **2004**;23(5):1125-35 doi 10.1038/sj.onc.1207023.
24. Lohoff M, Ferrick D, Mittrucker HW, Duncan GS, Bischof S, Rollinghoff M, *et al.* Interferon regulatory factor-1 is required for a T helper 1 immune response in vivo. *Immunity* **1997**;6(6):681-9 doi 10.1016/s1074-7613(00)80444-6.
25. Ogasawara K, Hida S, Azimi N, Tagaya Y, Sato T, Yokochi-Fukuda T, *et al.* Requirement for IRF-1 in the microenvironment supporting development of natural killer cells. *Nature* **1998**;391(6668):700-3 doi 10.1038/35636.
26. Penninger JM, Sirard C, Mittrucker HW, Chidgey A, Kozieradzki I, Nghiem M, *et al.* The interferon regulatory transcription factor IRF-1 controls positive and negative selection of CD8+ thymocytes. *Immunity* **1997**;7(2):243-54 doi 10.1016/s1074-7613(00)80527-0.
27. Fragale A, Gabriele L, Stellacci E, Borghi P, Perrotti E, Ilari R, *et al.* IFN regulatory factor-1 negatively regulates CD4+ CD25+ regulatory T cell differentiation by repressing Foxp3 expression. *J Immunol* **2008**;181(3):1673-82 doi 10.4049/jimmunol.181.3.1673.
28. Lee EJ, Jo M, Park J, Zhang W, Lee JH. Alternative splicing variants of IRF-1 lacking exons 7, 8, and 9 in cervical cancer. *Biochem Biophys Res Commun* **2006**;347(4):882-8 doi 10.1016/j.bbrc.2006.06.145.
29. Goedegebuure PS, Eberlein TJ. The role of CD4+ tumor-infiltrating lymphocytes in human solid tumors. *Immunol Res* **1995**;14(2):119-31 doi 10.1007/BF02918172.
30. Sultan M, Schulz MH, Richard H, Magen A, Klingenhoff A, Scherf M, *et al.* A global view of gene activity and alternative splicing by deep sequencing of the human transcriptome. *Science* **2008**;321(5891):956-60 doi 10.1126/science.1160342.
31. Martinez NM, Lynch KW. Control of alternative splicing in immune responses: many regulators, many predictions, much still to learn. *Immunol Rev* **2013**;253(1):216-36 doi 10.1111/imr.12047.

Figure Legends

Figure 1. The tumor microenvironment impacts CD4⁺ T-cell alternative splicing. (A) Left: Pattern of alternative splicing obtained by RNA-sequencing of CD4⁺ T cells from three spleens and two MC-38 tumors. Right: Types of alternative splicing patterns. (B) GSEA analysis of RNA-sequencing data of CD4⁺ T cells from spleens and MC-38 tumors. Geneset: reactome mRNA splicing. FDR, false-discovery rate. (C) Heatmap showing RNA-sequencing data of CD4⁺ T cells from spleens and MC-38 tumors. (D and E) Digital PCR analysis of (C) *Irf1* and (D) *Irf1Δ7* mRNA in Th1 cells differentiated for 1, 2, 4, and 24 hours. Results were normalized to the expression of mouse *Actb* (encoding β-actin). (F) Percentage of *Irf1* and *Irf1Δ7* mRNA detected by digital PCR (D-E). (G and H) RT-PCR analysis of *Irf1* (G) and *Irf1Δ7* (H) in sorted naïve CD4⁺ T, Th1, and Th2 cells. (I) Immunoblot analysis of IRF1 (antibody against N-terminal region) in Th1 cells differentiated for 24 hours. Results are shown as mean with SD of at least three representative and independent experiments (D-H). ****P*<0.001, *****P*<0.0001; one-way ANOVA (G and H).

Figure 2. TGFβ affects *Irf1Δ7* isoform appearance. (A) GSEA analysis of RNA-sequencing of CD4⁺ T cells from three spleens and two MC-38 tumors. Geneset: untreated CD4⁺ T cells vs. TGFβ-treated CD4⁺ T cells. (B) MA-plot showing RNA-sequencing of CD4⁺ T cells from spleens and MC-38 tumors (M: intensity ratio, A: average intensity). Genes upregulated or downregulated by at least 2-fold in CD4⁺ T cells from tumors compared with CD4⁺ T cells from spleens are labelled in red (Up) and blue (Down), respectively. Genes with similar expression in both conditions (NS) are labelled in black. TGFβ pathway-related genes are highlighted in yellow. (C) ELISA analysis of TGFβ in tumor shreds of different cell lines. (D and E) Nanopore sequencing of *Irf1* mRNA (D) exon (ratio) and (E) intron inclusion, relative to the total level of coverage for each condition, in naïve CD4⁺ T cells treated with IL12 and increasing doses of TGFβ (0, 10, 30 ng/mL) for 2 hours. (F-L) RT-PCR of *Irf1* (F), *Irf1Δ7* (G), *Irf1Δ7/Irf1* ratio (H), *Tbx21* (I), *Foxp3* (J), *Il12rb1* (K), and *Ifng* (L) mRNA in naïve CD4⁺ T cells treated with IL12 and increasing doses of TG-β (0, 1, 3, 10, and 30 ng/mL) for 2 hours (F-H) then replaced with a fresh medium containing IL12 during 24 hours (I-L). (M) RT-PCR of *Irf1Δ7/Irf1*

ratio mRNA in Th1 cells sorted from spleens and MC-38 tumors of mice from Supplementary Figure S8. (N) ELISA of IFN γ in tumor shreds of mice from Supplementary Figure S8. (O and P) Cytometry analysis of CD4⁺IFN γ ⁺ (L) and CD4⁺Foxp3⁺ cells isolated from spleens, lymph nodes (LN), draining-lymph nodes (DLN), and MC-38 tumors of mice treated as in Supplementary Figure S8. Results are shown as mean with SD or with SEM (K-L) of at least three representative and independent experiments. ns, not significant; * P <0.05, ** P <0.01, **** P <0.0001; Kruskal-Wallis test (C, F-L), one-way ANOVA (M), Mann-Whitney test (N-P).

Figure 3. The SFPQ splicing factor regulates *Irf1* pre-mRNA alternative splicing. (A) Heatmap showing RNA-sequencing of splicing factors in CD4⁺ T cells from three spleens and two MC-38 tumors. (B) Venn diagram of splicing factor genes upregulated in the TME (A) and *in silico* analysis of splicing factor binding sites on *Irf1* pre-mRNA sequence with AVISPA, ENCODE, SFmap, and RBPmap software. In brackets number of splicing factors binding sites detected. (C) RT-PCR of *HnrnpH*, *HnrnpF*, and *Sfpq* mRNA in naive CD4⁺ T cells treated with IL12 and TGF β (10 ng/mL) for 2 hours. (D) Left: Immunofluorescence of SFPQ (red) in naive CD4⁺ T cells treated or not with TGF β (10 ng/mL) for 2 hours. Nuclei were stained with the DNA-binding dye DAPI (blue). Scale bar, 6 μ m. Right: Mean fluorescence intensity (MFI), presented in arbitrary units (AU), and distance from α to ω in merged image at bottom right (line colors match staining in images). (E) GSEA analysis of RNA-sequencing data of CD4⁺ T cells from spleens and MC-38 tumors. Geneset: reactome PI3K/AKT activation. (F) RT-PCR of the *Irf1 Δ 7*/*Irf1* ratio in naive CD4⁺ T cells treated 1 hour with PI3K pharmacological inhibitor (LY-294002) and then differentiated into Th1 cells and treated or not with TGF β (10 ng/mL) for 2 hours. (G) RIP (mRNA immunoprecipitation) of SFPQ binding on *Irf1 Δ 7* mRNA. Results obtained with anti-SFPQ are presented in arbitrary units (AU) relative to those obtained with control immunoglobulin (Ig, isotype-matched control antibody). (H) RT-PCR of *Irf1 Δ 7* mRNA in Th1 cells differentiated for 2 hours in presence of TGF β from naive CD4⁺ T cells transfected with control siRNA or *Sfpq*-specific siRNA. Results are shown as mean with SD of at least

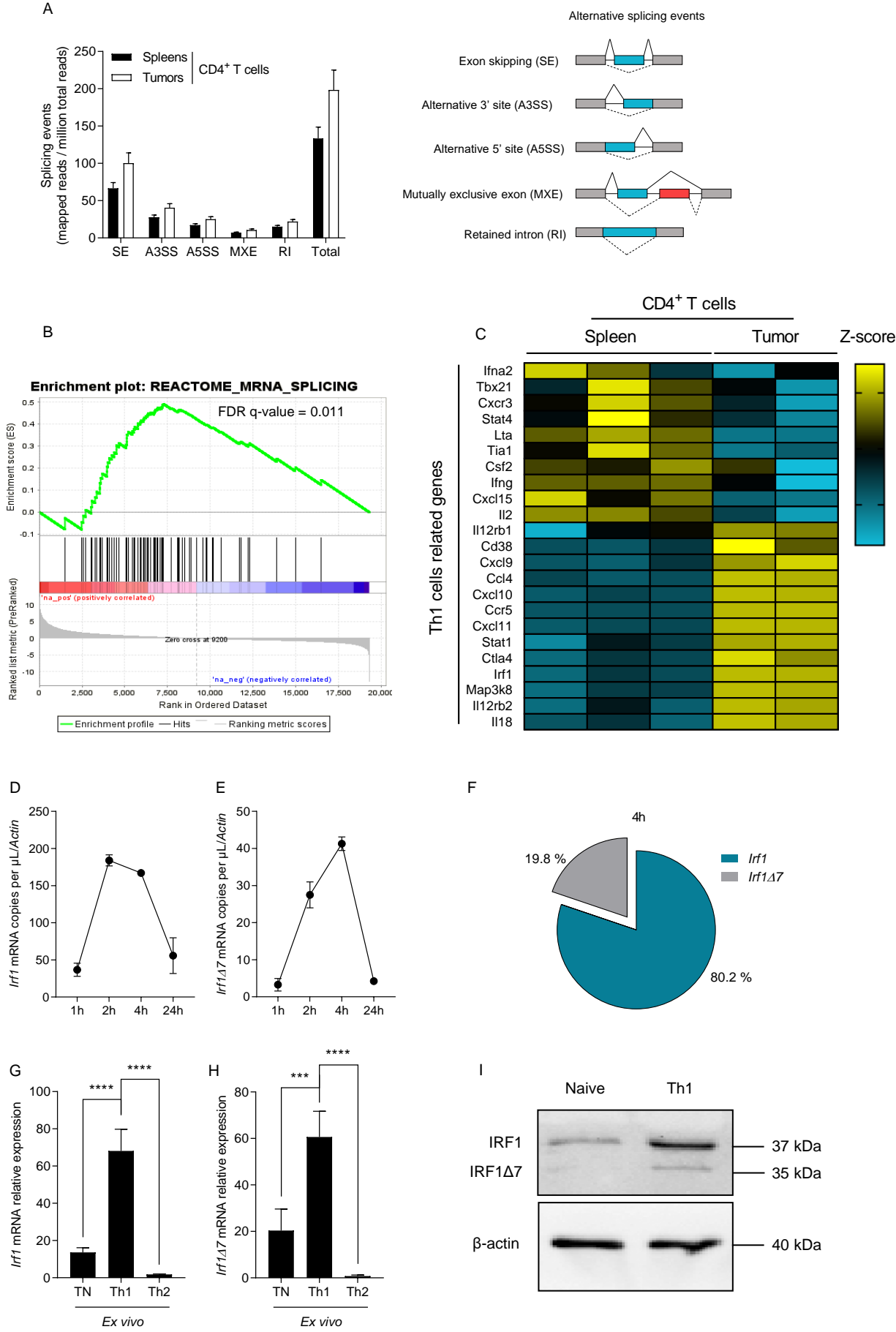
three representative and independent experiments. ns, not significant; * $P < 0.05$, ** $P < 0.01$, *** $P < 0.001$; Mann-Whitney test (C, D, H), One-way ANOVA (F, G).

Figure 4. IRF1 Δ 7 impairs Th1-cell activity. (A and B) RT-PCR analysis of *I12rb1* mRNA in Th1 cells differentiated for 24 hours from naive CD4⁺ T cells transfected with control siRNA (Ctrl), *Irf1*- *Irf1 Δ 7*-, or *Sfpq*-specific siRNA. (C and D) RT-PCR of *Ifng* mRNA in Th1 cells differentiated for 24 hours from naive CD4⁺ T cells transfected with control siRNA, *Irf1*-, *Irf1 Δ 7*- or *Sfpq*-specific siRNA. (E) ELISA of IFN γ in Th1 cells differentiated 72 hours from naive CD4⁺ T cells transfected with control siRNA, *Irf1*-, *Irf1 Δ 7*-, or *Sfpq*-specific siRNA. (F-H) RT-PCR of (F) *Irf1 Δ 7*, (G) *I12rb1*, and (H) *Ifng* mRNA in GFP⁺ cells sorted from naive CD4⁺ T cells 48 hours after retroviral infection with an empty-GFP vector (EV) or IRF1 Δ 7-GFP-overexpressing vector and differentiated for 72 hours into Th1 cells. (I- J) Cytometry analysis of (I) IFN γ ⁺GFP⁺ cells and (J) ELISA of IFN γ in the supernatant of Th1 cells treated as in (F-H). (K) ChIP analysis of the binding of IRF1 and short to the putative binding site at position -85 -72 of the *I12rb1* promoter in 293T cells transfected with a vector encoding *I12rb1* promoter, and vectors encoding for IRF1 and IRF1 Δ 7 both tagged with histidine and YFP. Results obtained with anti-histidine and anti-YFP are presented in arbitrary units (AU) relative to those obtained with control immunoglobulin (Ig, isotype-matched control antibody). (L) Transactivation of *I12rb1* promoter by IRF1 and short. *I12rb1* promoter reporter plasmids were transfected into 293T cells with vectors encoding IRF1 and short with different combinations. (M) FLIM-FRET in 293T cells transfected with IRF1-YFP and IRF1 Δ 7-CFP. Results are shown as mean with SD or with SEM (K) of at least three representative and independent experiments. ns, not significant; * $P < 0.05$, ** $P < 0.01$, *** $P < 0.001$, **** $P < 0.0001$; Kruskal-Wallis test (A, B, E, K, L), Mann-Whitney test (C, D, F-J, M).

Figure 5. IRF1 Δ 7 is present in human Th1 cells and modulates their activity. (A) RT-PCR of *Irf1 Δ 7* mRNA in naive CD4⁺ T cells isolated from three human blood donors or after 1 hour of differentiation into Th1, Th2, Th17 cells. (B) RT-PCR of *Irf1 Δ 7* mRNA in naive CD4⁺ T cells and Th1, Th2, Th17 cells

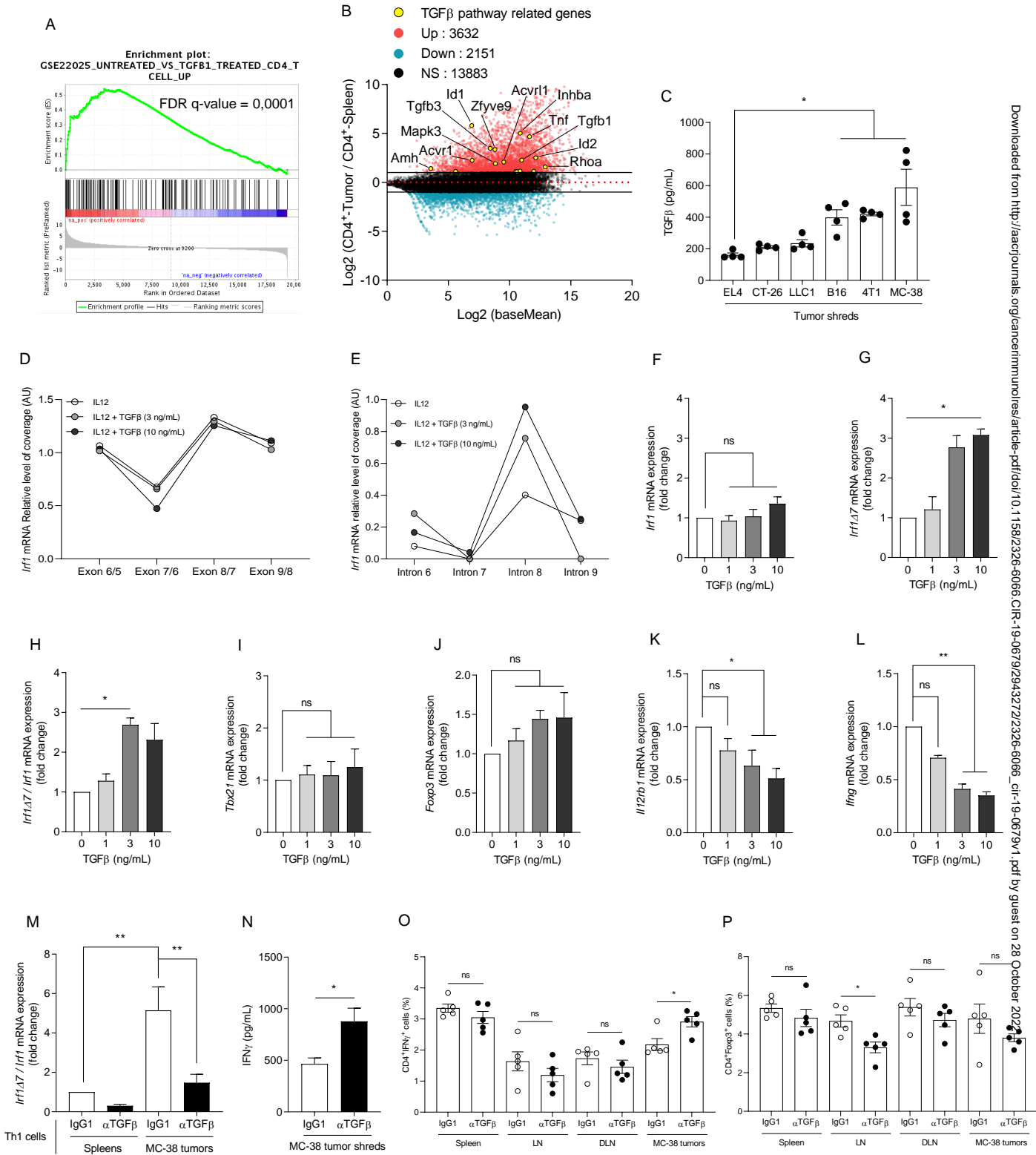
isolated from three human blood donors and sorted by flow cytometry. (C and D) RT-PCR of (C) *IL12RB1* and (D) *IFNG* mRNA in Th1 cells differentiated for 24 hours from naive CD4⁺ T cells isolated from six human blood donors and transfected with control siRNA or *Irf1Δ7*-specific siRNA. (E and F) IFN γ intracellular staining (E) and ELISA (F) of IFN γ protein in supernatants in Th1 cells differentiated for 72 hours from naive CD4⁺ T cells isolated from three human blood donors and transfected with control siRNA or *Irf1Δ7*-specific siRNA. (G-N) RT-PCR of *IRF1* (G and H), *IRF1Δ7* (I and J), and *IRF1Δ7/IRF1* (K and L) ratio, and *IFNG* (M and N) mRNA in naive CD4⁺ T cells (G, I, K, M) and *ex vivo* (H, J, L, N) Th1 cells isolated from three human blood donors and treated with increasing doses of TGF β (0, 1, 3, 10, and 30 ng/mL) for 1 hour (G-L) and then cultured with IL12 and anti-IL4 blocking antibody for 24 hours (M-N). (O) RT-PCR of the *Irf1Δ7/Irf1* ratio mRNA in Th1 cells sorted from four healthy donors and four patients (colorectal tumor). Results are shown as mean with SD of at least three representative and independent experiments. ns, not significant; * P <0.05, ** P <0.01, *** P <0.001; one-way ANOVA (A, B), Mann-Whitney test (C-F, O), Kruskal-Wallis test (G-N).

Figure 1: The tumor microenvironment impacts CD4⁺ T cell alternative splicing



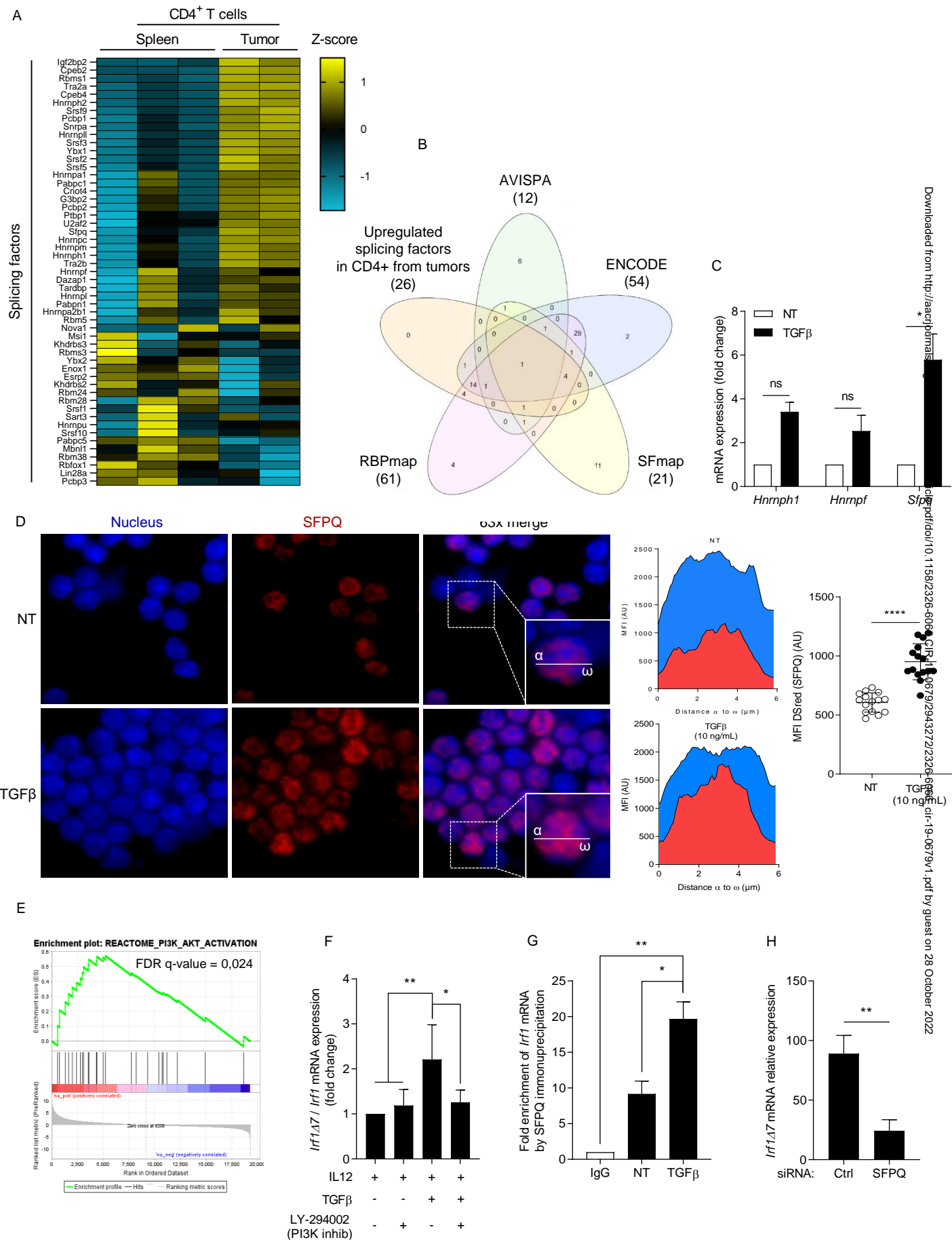
Downloaded from <http://aacrjournals.org/cgi/journal/doi/10.1158/2326-6066.CCR-19-0679V1> by guest on 28 October 2022

Figure 2: TGFβ affects *Irf1Δ7* isoform appearance



Downloaded from <http://aacrjournals.org/cancerimmunolres/article-pdf/doi/10.1158/2326-6066.CCR-19-0679V1> by guest on 28 October 2022

Figure 3: SFPQ splicing factor regulates *Irf1* pre-mRNA alternative splicing



Downloaded from http://aacrjournals.aacrjournals.org/ on 10/28/22. See all uses for https://pubs.aacr.org/journal-aacrrjournals/doi/10.1158/2326-6066.CCR-22-0679.1

Figure 4: IRF1Δ7 impairs Th1 cells activity

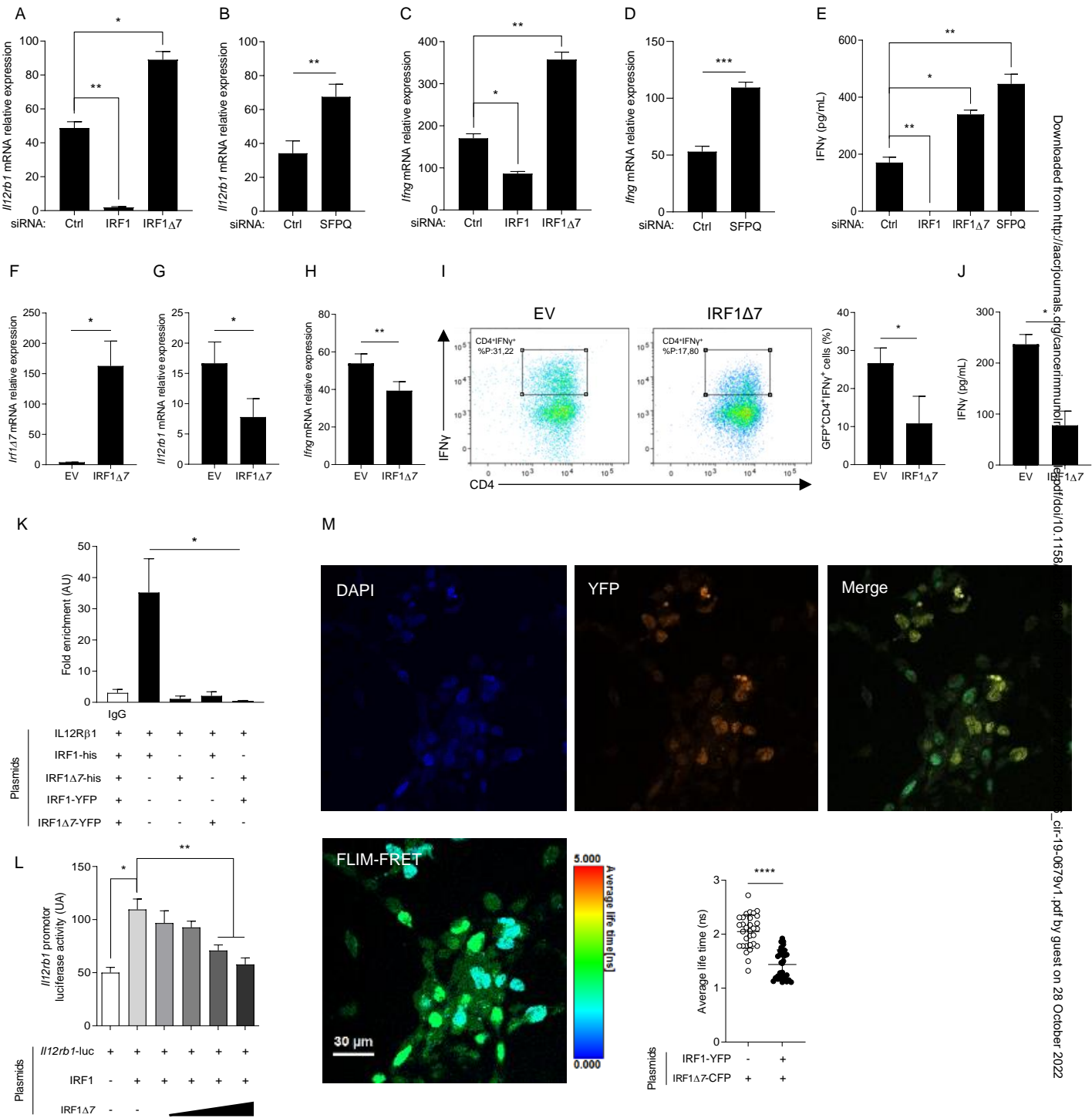


Figure 5: IRF1 Δ 7 is present in human Th1 cells and modulates their activity

